Remote Sensing of Environment 210 (2018) 48–64

Contents lists available at ScienceDirect

Remote Sensing of Environment

journal homepage: www.elsevier.com/locate/rse

Support vector regression snow-depth retrieval algorithm using passive microwave remote sensing data

Xiongxin Xiao[a], Tingjun Zhang[a,*], Xinyue Zhong[b], Wanwan Shao[a], Xiaodong Li[a]

[a] Key Laboratory of Western China's Environmental Systems (Ministry of Education), College of Earth and Environment Sciences, Lanzhou University, Lanzhou 730000, China

[b] Northwest Institute of Eco-Environment and Resources, Chinese Academy of Sciences, Lanzhou 730000, China

ARTICLE INFO

Keywords:
Snow-depth retrieval
Snow cover stage
Land cover
Topography
Eurasia

ABSTRACT

Snow cover is an informative indicator of climate change because it can affect local and regional surface energy and water balance, hydrological processes and climate, and ecosystem function. Passive microwave (PM) remote sensing data have long been used to retrieve snow depth and snow water equivalent with large uncertainties. The objective of this study is to develop snow-depth retrieval algorithm based on support vector regression (SVR) technique using PM remote sensing data and other auxiliary data. Ground-based daily snow depth data from 1223 stations across Eurasian continent were used to construct and validate the snow-depth retrieval algorithm. This SVR snow-depth retrieval algorithm partitioned three snow cover stages, and four land cover types then generated twelve snow-depth models for each phases. A non-linear regression method based on support vector regression (SVR) was used to retrieve snow depth with PM brightness temperatures, location (latitude and longitude), and terrain parameters (elevation) as input data and land cover as auxiliary data. In addition, we compared the performance of the SVR snow-depth retrieval algorithm with four alternative algorithms: the Chang algorithm, the Spectral Polarization Difference (SPD) algorithm, the Artificial/Neural Networks (ANN) and, an algorithm based on linear regression. Comparing results obtained from these five snow-depth retrieval algorithms against the ground-based daily snow depth data, the SVR snow-depth retrieval algorithm performs much superior with reduced uncertainties. We report the results aimed at evaluating the impact of the variation of snow cover stages and land cover types. The preliminary results suggest that the SVR snow-depth algorithm could detect deep snow with high accuracy and decrease the impact of saturation effects. These results suggest that the SVR snow-depth retrieval algorithm integrating PM remote sensing data and other auxiliary data (land cover types, location, terrain, snow cover stage with indirectly considering grain size variation) can be a more efficient and effective algorithm for retrieving snow depth and snow water equivalent over various scales.

1. Introduction

Snowmelt is an important water source for rivers and lakes. Seasonal snow and glaciers store large amounts of freshwater and are critical for water cycles, hydrology, climatology and water management (Armstrong and Brodzik, 2002; Immerzeel et al., 2010; Robinson and Frei, 2000; Tedesco et al., 2014; Tedesco and Narvekar, 2010; Wang et al., 2015). Snow cover has important implications for energy exchange processes between the land and atmosphere because of its high surface albedo and consequent thermodynamic processes in winter (Cohen and Entekhabi, 2001; G.Barry and Gan, 2011; Gong et al., 2007; Hall et al., 2014). In addition, snow cover has a significant influence on soil thermal regime (Goodrich, 1982; Zhang, 2005; Zhang et al., 1996), winter soil CO_2 efflux, soil carbon and soil nitrogen mineralization, tundra vegetation composition and canopy structure (Schimel et al., 2004; Sturm et al., 2005; Tape et al., 2006; Welker et al., 2000). Both in situ and satellite observational records show that the Northern Hemisphere snow cover extent has significantly reduced in the past 90 years (IPCC AR5, 2013).

Due to the heterogeneity of snow properties in spatiotemporal distribution, conventional snow measurements lack the ability to capture the spatial and temporal variability snow characteristic. Satellite observations provide an effective approach to monitor snow cover with continuous observations and global coverage. Passive Microwave (PM) remote sensing has become an efficient method to estimate snow depth and snow water equivalent, as it provides more information of spatiotemporal snowpack variation. Snow physical properties, including snow depth, snow water equivalent, liquid-water content, grain size, density

* Corresponding author.
E-mail addresses: xiaoxx15@lzu.edu.cn (X. Xiao), tjzhang@lzu.edu.cn (T. Zhang), xyzhong@lzb.ac.cn (X. Zhong), shaoww09@lzu.edu.cn (W. Shao), lixd16@lzu.edu.cn (X. Li).

https://doi.org/10.1016/j.rse.2018.03.008
Received 16 August 2017; Received in revised form 27 February 2018; Accepted 5 March 2018
Available online 16 March 2018
0034-4257/ © 2018 Elsevier Inc. All rights reserved.

and stratification among others, exhibit substantial temporal and spatial variability (Hall, 1987; Rosenfeld and Grody, 2000). Microwave remote sensing observation is based on the thesis that snow-emitted microwave radiation has a strong dependence on snow physical properties, besides snow depth, mainly on snow density, grain size, and stratification (Rosenfeld and Grody, 2000). PM brightness temperature data reflects snowpack scattering information in terms of the combined effect of snow density, liquid water content, snow metamorphism, and grain size, which also affect the dielectric properties of snowpack. Changes in snow property directly affect microwave brightness temperature. Snow depth is positively related to volumetric scattering of microwave radiation and negatively related to measured brightness temperature from satellite microwave sensors (Gan et al., 2013). Moreover, Zhong et al. (2014) found that snow density is positively related to latitude and negatively related to elevation based on ground-based daily snow depth data. Studies also demonstrated that topographic factors play a critical role in snow distribution and snow physical properties (Bi et al., 2015; Gharaei-Manesh et al., 2016; Li et al., 2015; Savoie et al., 2009; Smith and Bookhagen, 2016). Snow cover products obtained from PM remote sensing data have been widely applied to investigate regional and global climate change, and validate hydrological and climate models (Brown and Robinson, 2011; Brown and Mote, 2009; MacKay et al., 2003). In contrast with visible and thermal infrared bands, PM radiation can probe through clouds and interact with snowpack providing dual polarization data at different frequencies (Chang et al., 1987; Che et al., 2008; Liang et al., 2015; Tait, 1998; Tedesco et al., 2004).

To quantify and model the snowpack, it is necessary to account for spatial differences in snow cover over different land cover types. Because vegetation overlaying snow attenuates its microwave scatter signal, underlying land cover adds to the complications of estimating snow depth and snow water equivalent from PM data (Che et al., 2016; Foster et al., 1999; Yu et al., 2012). Vander Jagt et al. (2013) pointed out that microwave signal sensitivity to snow depth was reduced by 23–63% due to the presence of vegetation in some places. To reduce the effect of forest cover, the forest fraction was included to derive snow depth and snow water equivalent (Che et al., 2008; Foster et al., 1997). Additionally, attenuation of passive radiation between snow depth or snow water equivalent and different land cover types are both pronounced and different. Goïta et al. (2003) developed different algorithm according to different land cover types. Romanov and Tarpley (2007) improved the snow depth retrieval algorithm and accounted for tree cover fraction and the tree types (deciduous or coniferous).

There have been several algorithms developed to estimate snow depth and snow water equivalent using PM brightness temperature data (Aschbacher, 1989; Chang et al., 1987; Che, 2006; Che et al., 2008; Grippa et al., 2004; Kelly, 2009; Kelly et al., 2003; Rott and Aschbacher, 1989; Takala et al., 2011; Tedesco et al., 2004). Typically, most snow-depth retrieval algorithms were developed using the difference between horizontal polarized brightness temperatures of 19 (or 18) GHz and 37 GHz. However, recent studies have shown that snow-depth retrieval algorithms using brightness temperatures from other channels, such as ~10 GHz (Derksen, 2008) and 85 GHz (Kelly, 2009), may better resolve shallow snow cover and be less sensitive to saturation of microwave signal at 19 GHz (Kelly, 2009; Smith and Bookhagen, 2016; Tedesco and Narvekar, 2010). PM brightness temperatures are available on Advanced Microwave Scanning Radiometer for Earth Observing System (AMSR-E), the Advanced Microwave Scanning Radiometer 2 on the Global Change Observation Mission – Water (GCOM-W AMSR2), the Special Sensor Microwave Imager (SSM/I) and the Special Sensor Microwave Imager Sounder (SSMIS). Most snow-depth retrieval algorithms were employed based on the notion that PM brightness temperature differences between 18 and 37 GHz may reflect snow depth and snow water equivalent (Chang et al., 1987). These retrieval algorithms tend to underestimate snow depth and snow water equivalent (Basak et al., 2007; Gan et al., 2013). Meanwhile, new modeling approaches (e.g. artificial neural networks, support vector regression, decision tree) are emerging (Gharaei-Manesh et al., 2016). These new approaches are intended to replace traditional linear methods and to explore, using data-mining, non-linear functional relationships between input (brightness temperatures) and output (snow depth) variables. Knowledge of snowpack physical processes is not necessary for these modeling approaches. Tedesco et al. (2004) applied ANN to estimate snow water equivalent and snow depth. Liang et al. (2015) in their study used a Support Vector Machine (SVM) integrating PM brightness temperature and visible reflectance to retrieve snow depth and snow water equivalent. However, there are still limitations for those methods due to the complexity of topography, heterogeneous land cover types which attenuate microwave scatter signal.

The primary goal of this study is to develop a support vector regression (SVR) snow-depth retrieval algorithm using PM remote sensing data and related auxiliary datasets. The developed SVR snow-depth retrieval algorithm accounts for three snow cover stages and four land cover types (forest, shrub, prairie and bare-land). In Section 2, we introduce data for the SVR snow-depth retrieval algorithm over the Eurasian continent. In Section 3, we describe the process of snow depth retrieval and methods used at each step. Following this approach, we use the SVR snow-depth retrieval algorithm to estimate snow depth across Eurasian continent and evaluate the algorithm performance against the in situ measured daily snow depth data. We also run five other existing snow-depth retrieval algorithms against the same in situ measured daily snow depth data for algorithm comparison.

2. Data

Snow accumulation (snow depth) is heterogeneous and some secondary forces (such as wind, avalanche, land cover etc.) may redistribute snow and change snow condition. Previous studies have shown that snow depth has a close relationship with PM brightness temperature in different channels, and brightness temperature difference increases with snow depth (Aschbacher, 1989; Chang et al., 1987; Che, 2006; Che et al., 2008). Moreover, previous studies have demonstrated that many factors or parameters influence snow physical properties and the distribution of snow cover including, but not limited to, vegetation (Che et al., 2016; Derksen et al., 2005; Foster et al., 1997), near-surface soil temperature and air temperature (Grippa et al., 2004; Josberger and Mognard, 2002; Singh and Gan, 2000), snow grain size and snow density (Dai et al., 2012), elevation (Savoie et al., 2009), geographic location and time of day (Sturm et al., 2010), wind speed and topographic relief (Smith and Bookhagen, 2016). In this study, we propose the following formulas (Eqs. (1) and (2)) to describe snow depth and snow water equivalent retrieval processes:

$$[DS] = F(A, T, G, L, S, D...) + \varepsilon \quad (1)$$

in which, F ( ) denotes the transformation function. DS is the digital signal from remote sensing sensor (PM, active microwave, visible spectral remote sensing etc.). A is the atmosphere (wind speed, air temperature, humidity, precipitation etc.). T is the topography (elevation, terrain slope, aspect etc.). G is the ground (ground surface temperature, vegetation type etc.). L is the location (latitude, longitude). S is the snow properties (snow grain size, density, reflectance, snow depth, snow water equivalent etc.). D is the day of year. ε is residual error or uncertainty (uncertainty between sensor signal and measured snow properties).

Using the parameters (A, T, G, L, S, D …) to yield DS, is called the snow forward process (Eq. (1)). For example, Forman and Reichle (2015) used snow property parameters (S), which includes snow water equivalent, density and snow temperature, near-surface air temperature (A), soil and vegetation temperature (G) as input parameters of SVM approach (F(·)) to estimate PM brightness temperatures. Contrarily, when DS and other parameters (A, T, G, L, D …) are used to generate estimated value of snow parameters (e.g. snow depth), this process is

called the snow retrieval process. Eq. (2) describes the snow retrieval process.

$$[S] = g(A, T, G, L, DS, D...) + \varepsilon \quad (2)$$

where the g ( ) denotes the retrieval function. For example, we usually get snow depth (S) integrating PM data (DS) and linear regression method (g (·)). Most studies have focused on retrieving snow depth and snow water equivalent. The difference among those snow retrieval algorithms is the parameters used or effect factors considered (such as grain size, density, land cover and topography) and the retrieval function.

We offer a new perspective on snow depth retrieval by using three channels of PM brightness temperature (19 GHz, 37 GHz and 85 (or 91) GHz) with vertical and horizontal polarizations and other parameters including land cover types (G), day of year (D), latitude, longitude and, elevation (T). The main method (retrieval function) for deriving snow depth on the Eurasian continent also uses non-linear regression (SVR). This regression approach has also been used in Liang et al. (2015) study. The detailed information for SVR method can be found in many published papers (Basak et al., 2007; Gunn, 1998; Smola and Vapnik, 1997; Welling, 2004) and will be describe in Section 3. We will describe the datasets we used in detail, including the observed snow depth from meteorological stations, PM brightness temperature data, land cover products, and topographic data.

2.1. Ground-based measurements

Daily measured snow depth was used to construct and validate the SVR snow-depth retrieval algorithm. Ground-based measurements of daily snow depth were obtained from 1223 meteorological stations across the Eurasian continent (Fig. 1). This includes daily measured snow depth data from 635 Chinese meteorological stations, the National Meteorological Information of China Meteorological Administration (Zhong, 2014). Daily snow depth datasets include snow depth, measurement time, and location information. Regular snow depth measurements have been conducted at Russian Hydrometeorological stations since 1882 (Bulygina et al., 2011). The former Soviet Union (USSR) daily snow depth datasets are from the All-Russian Research Institute for Hydrometeorological Information-World Data Center (RIHMI-WDC) that has a total of 551 Hydrometeorological stations in the former USSR (Zhong et al., 2014). Before being stored at the RIHMI-WDC, the former USSR meteorological datasets have been quality controlled (Veselov, 2002). Mongolia daily snow datasets from the National Snow and Ice Data Center (NSIDC), University of Colorado Boulder includes daily snow depth and snow cover days (Zhong, 2014). Mongolian datasets include 37 meteorological stations. Table 1 summarizes the detail of meteorological stations across Eurasia.

Table 1
Sources of snow data across Eurasia.

Country	No. of sites	Time span	Source
China	635	1957–2013	Chinese Meteorological Data Sharing Center (CMDC), http://data.cma.cn/en
Soviet Union (USSR)	551	1914–2012	RIHMI-WDC, www.meteo.ru
Mongolia	37	1969–2001	NSIDC, http://nsidc.org/

2.2. Passive microwave brightness temperature data set

The PM brightness temperature (Tb) data have been gridded into the equal-area scalable earth grid (EASE-Grid) (Brodzik and Knowles, 2002). The SSM/I (Armstrong et al., 2008) data from 1987 to 2008 and SSMIS data from December of 2006 to present from F17 satellite (Dai et al., 2015; Sun and Weng, 2008; Wentz, 2013) from NSIDC were acquired daily in three EASE-Grid projection (Northern Hemisphere azimuthal, Southern Hemisphere azimuthal, and global cylindrical), with a normal resolution of 25 × 25 km^2 (Armstrong and Brodzik, 1995; Armstrong et al., 2008). SSM/I and SSMIS sensors are mounted

Fig. 1. Distribution of meteorological stations across Eurasian continent. Background indicates elevation variation.

Table 2
Detail description of SSM/I and SSMIS sensors. H and V denote horizontal and vertical polarization, respectively.

Satellite	SSM/I			SSMIS
Platform	F08	F11	F13	F17
Temporal coverage	1987.7–1991.12	1991.12–1995.5	1995.5–2008.6	2006.12–present
Descending node (decimal hours)	18.20	5.17	5.58	5.31
Channels (GHz)	19H, V; 22V; 37H, V; 85H, V			19H, V; 22V; 37H, V; 91H, V

on a United States Defense Meteorological Satellite Program satellite. These measurements contain four channels (19, 22, 37 and 85 (or 91) GHz) with orthogonal polarization. An exception is the 22 GHz channel that is only vertically polarized. We also used descending orbit brightness temperature data, because of the likelihood of liquid water in snowpack during afternoon satellite overpass (Derksen et al., 2000). Table 2 summarizes the details of passive microwave remote sensors over different satellites.

2.3. MODIS land cover

The snow redistribution and snow microwave emissions are influenced by heterogeneous land cover types (Che et al., 2014; Yu et al., 2012). When developing the SVR snow-depth retrieval algorithm, we used land cover type from MODIS land cover products (MCD12Q1) captured during 2001 to 2013, following the Boston University International Geosphere–Biosphere Program (IGBP) classification scheme (Friedl and Sulla-Menashe, 2011; Friedl et al., 2010; Hansen et al., 2003; Strahler et al., 1999). Seventy-six tiles of land cover type products are required to cover the whole Eurasia continent. In this study, we only consider four kinds of land cover (forest, shrub, prairie and bare-land) to drive snow depth. Moreover, we reclassified the IGBP global vegetation classification scheme to six classes including water, forest, prairie, shrub, bare-land and unclassified (Fig. 2). Section 3 showed more details about reclassification rules.

2.4. Topographic data

To consider the impact of terrain parameters (e.g. elevation) on snow-depth retrieval modeling, topographic data were used as auxiliary data. The ETOPO1 (Amante and Eakins, 2009) were used as topographic data, and it is available at http://www.ngdc.noaa.gov/mgg/global/. The elevation of meteorological stations was directly obtained from the ETOPO1 data (Fig. 1).

3. Methods: theoretical basis for snow depth retrieval

The flowchart of the proposed snow-depth retrieval algorithm (Fig. 3) can be described in six steps:

Step 1. Data preparation

Primary datasets for this study include PM brightness temperatures (i.e. Tb19V, Tb19H, Tb37V, Tb37H, Tb85V (or Tb91V) and Tb85H (or

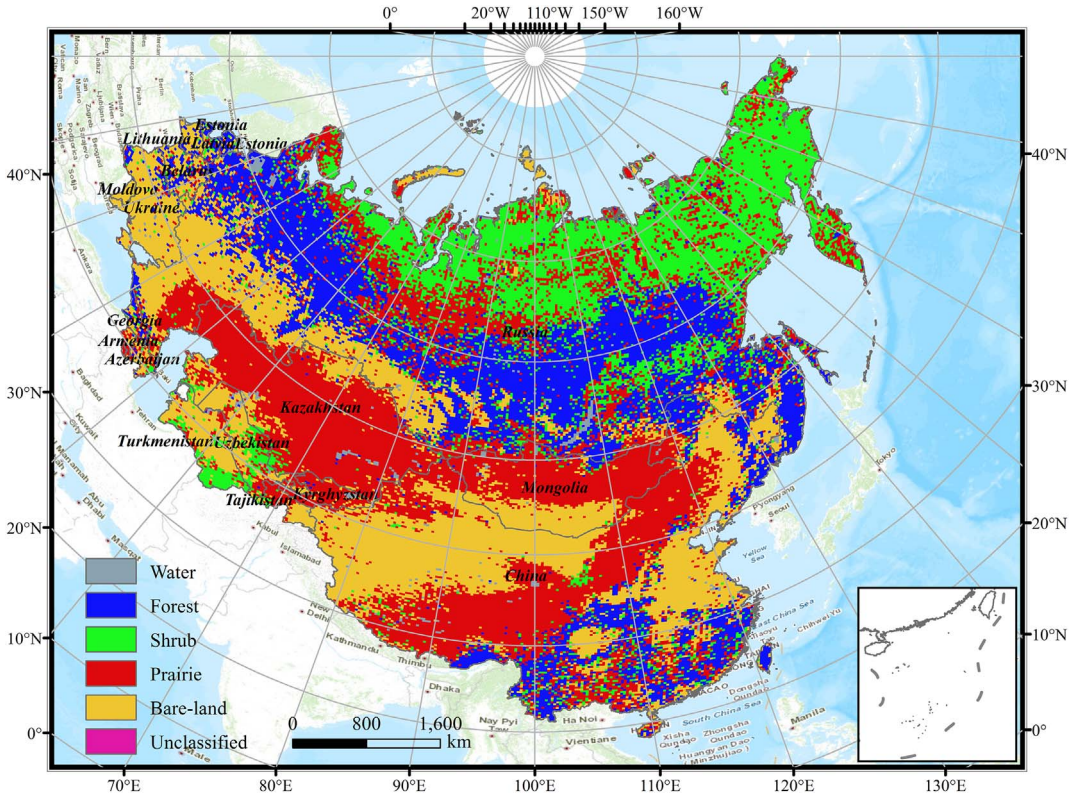

Fig. 2. The IGBP land cover classification were reclassified into six classes (water, forest, shrub, prairie, bare-land and unclassified), MODIS land cover product (MCD12Q1) of 2010 as an example.

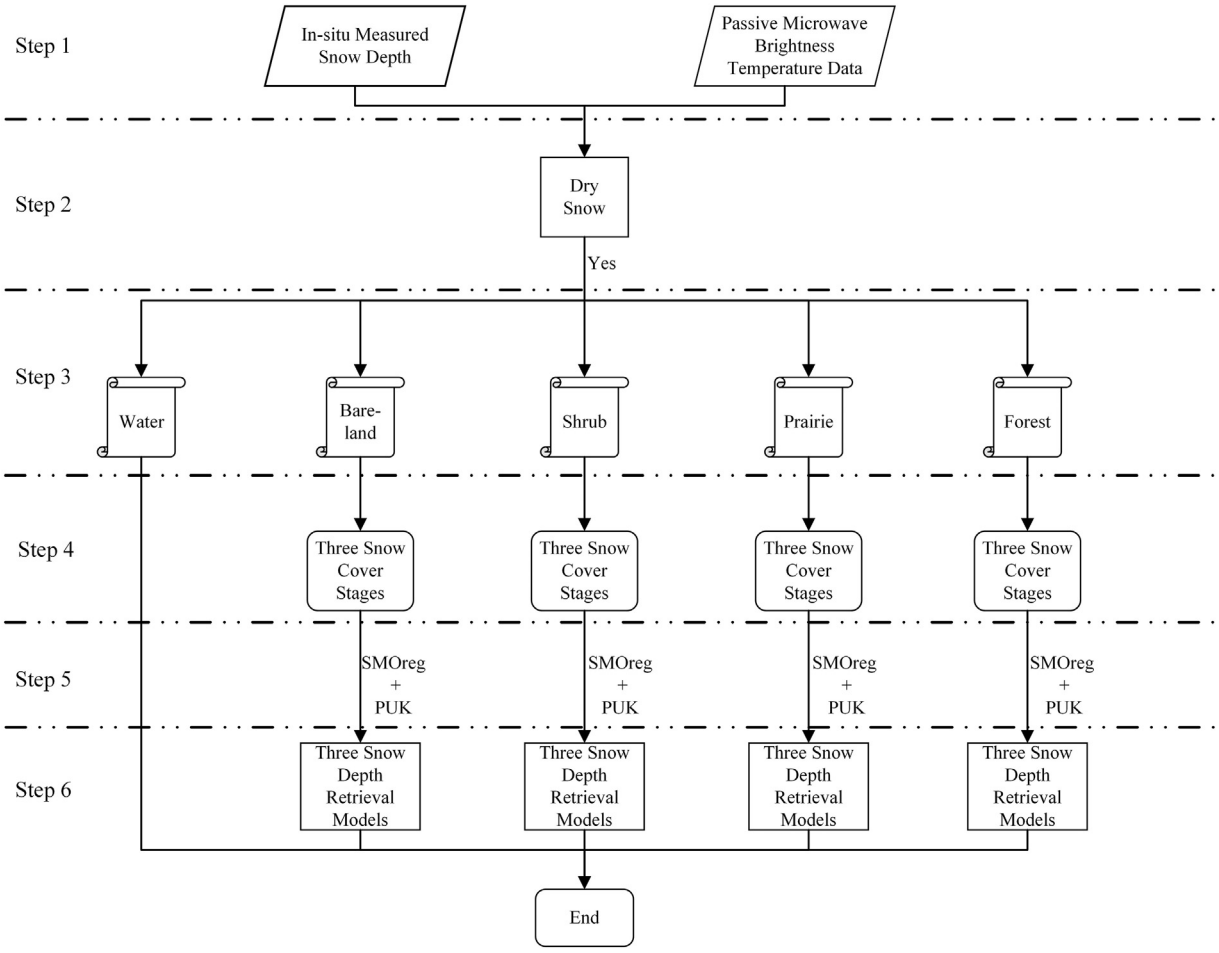

Fig. 3. Flowchart of the proposed retrieval algorithm for estimating snow depth.

Table 3
Steps to distinguish snow from precipitation, cold desert, and frozen ground. K is unit, Kelvin.

Steps	Conditions for SSM/I	Conditions for SSMIS
1. Scattering signature	(Tb19V–Tb37V) > 0 K or (Tb22V–Tb85V) > 0 K	(Tb19V–Tb37V) > 0 K
2. Precipitation	Tb22V ≥ 259 K or (254 ≤ Tb22V ≤ 258 K and (Tb19V–Tb37V) ≤ 2 K)	Tb22V ≥ 259 K or (254 ≤ Tb22V ≤ 258 K and (Tb19V–Tb37V) ≤ 2 K)
3. Cold deserts	(Tb19V–Tb19H) ≥ 18 K and (Tb19V–Tb37V) ≤ 10 K and (Tb37V–Tb85V) ≤ 10 K	(Tb19V–Tb19H) ≥ 18 K and (Tb19V–Tb37V) ≤ 10 K
4. Frozen ground	(Tb19V–Tb19H) ≥ 8 K and (Tb1 9 V - Tb3 7 V) ≤ 2 K and (Tb22V–Tb85V) ≤ 6 K	(Tb1 9 V -Tb19H) ≥ 8 K and (Tb19V–Tb37V) ≤ 2 K

Tb91H)) and ground-based measured snow depth. Section 2.2 describes the details of PM brightness temperature data. In addition, many other parameters were needed as input data such as the measured snow depth location and terrain parameters (latitude, longitude, elevation).

Step 2. Dry snow identification

The microwave radiation characteristics of snow cover is similar to that of precipitation, cold deserts and, frozen ground (Grody and Basist, 1996). Grody and Basist (1996) established a decision tree to remove the scattering signatures associated with cold deserts, cold rain and frozen ground that can inhibit the true detection of snow cover (Table 3). To make full use of SSMIS brightness temperature data, which does not have 85 GHz channel, we removed the criteria that included 85 GHz channels (Che et al., 2008).

Due to the existence of wet snow, estimates of snow depth and snow water equivalent by microwave radiation is hindered. With increasing liquid water content of the snow medium, the absorption of microwave radiation will dominate volume scattering (Hallikainen, 1989). To employ a snow-depth retrieval algorithm with higher accuracy, we have found it necessary to separate PM data that measured snowpack affected by wet snow or deep hoar. The SVR snow-depth retrieval algorithm applied the following dry snow criteria to remove wet snow (Goodison et al., 1986; Singh and Gan, 2000; Walker and Goodison, 1993):

$$Tb37V < 250\ K$$

$$Tb19V - Tb37V \geq 9\ K$$

$$Tb37V - T37bH \geq 10\ K$$

$$P_{factor} = \frac{Tb37V - Tb37H}{Tb37V + Tb37H},\ Pfactor > 0.026$$

These criteria were used to establish dry snow condition. Additional criteria also used in dry snow conditions included the P_factor < 0.041 for DMSP-F10 and DMSP-F13.

Step 3. Reclassification of land cover categories

In this study, we used MODIS MCD12Q1 yearly data with the IGBP global vegetation classification scheme as auxiliary data to drive snow depth. There are 17 types in the IGBP classification system (Table 4). In

Table 4
Accuracy of 24 snow-depth retrieval models with R, MAE, RMSE, MARE.

Phase	Stage	Land cover	R	MARE/%	MAE/cm	RMSE/cm	Model code
2001–2006	i	Forest	0.73	74.88	8.85	13.62	1
		Shrub	0.72	65.69	5.99	8.66	2
		Prairie	0.82	62.88	5.57	8.88	3
		Bare-land	0.69	69.87	3.55	6.05	4
	ii	Forest	0.79	40.20	7.80	11.16	5
		Shrub	0.77	48.57	8.36	11.97	6
		Prairie	0.85	61.92	6.57	10.56	7
		Bare-land	0.79	65.08	6.26	9.54	8
	iii	Forest	0.82	62.61	12.06	17.04	9
		Shrub	0.83	67.57	10.59	15.35	10
		Prairie	0.90	68.05	9.35	14.83	11
		Bare-land	0.75	89.36	9.51	14.36	12
2007–2012	i	Forest	0.81	54.81	5.63	9.08	13
		Shrub	0.73	55.25	5.60	9.98	14
		Prairie	0.83	51.66	7.81	7.82	15
		Bare-land	0.79	58.19	2.23	4.02	16
	ii	Forest	0.81	46.51	8.17	11.33	17
		Shrub	0.84	47.82	7.37	10.72	18
		Prairie	0.88	64.04	5.40	9.37	19
		Bare-land	0.82	58.15	5.34	8.38	20
	iii	Forest	0.80	69.73	11.20	15.81	21
		Shrub	0.84	59.77	9.88	14.91	22
		Prairie	0.90	73.38	7.72	13.58	23
		Bare-land	0.82	75.05	8.35	13.47	24

the SVR snow-depth retrieval algorithm, we reclassified the original MODIS land cover types classes into six classes (Fig. 3; Table B, in the Appendix A). A similar reclassification rule was also used by Bin (2013) to improve the PM snow retrieval algorithm over Qinghai-Tibet Plateau. Based on previous studies (Bin, 2013; Che et al., 2016; Foster et al., 1997; Yu et al., 2012) associated with vegetation and snowpack, we applied these four land cover types (forest, prairie, shrub, and bare-land) to establish snow-depth retrieval models.

Step 4. Snow cover year and stages

To explore snow properties and establish the snow-depth retrieval model between same stages of different years, we used snow cover stage and snow cover year in this study. We defined snow cover year as the period between July of a given year (t-1) and June of the following year (t). Then we divided snow cover year into three stages: snow cover accumulation stage, snow cover stabilization stage (Huang et al., 2007; Zhong et al., 2014), and snow cover ablation stage. The snow cover accumulation stage extends from September to November during which time new/fresh snow appears (coded, i). From the previous year (t-1), December to the current February (t) is the snow cover stabilization stage (coded, ii) because the properties of snow change slowly. The snow cover ablation stage ranges from March to June; the time during which snow begins to melt and its properties show obvious fluctuation (coded, iii) (Zhong et al., 2014).Through these definitions, we may not be able to account for grain size and density variations on short-term (hourly) fluctuations but it is possible to account for stage variations.

Step 5. Retrieval model based on regression technique

The SVR method developed by Vapnik et al. (1997) relies on establishing a regression function (Üstün et al., 2005).

$$f(x) = w^T x + b \quad (w, x \in R^d) \tag{3}$$

where w and b are slope and offset of the regression function f(x), d is dimensional input space. For a more detailed description the reader should refer to Üstün et al. (2005), Smola and Vapnik (1997).

The SVR method attempts to find snow depth f(x) as a function of the input object x (spectrum, brightness temperature, station coordinate and others) (Üstün et al., 2006). Selecting a suitable kernel function is significant to model complex non-linear relationships for SVR. We complete this experiment with Pearson VII universal function kernel (PUK) (Üstün et al., 2006) as the kernel and the improved sequential minimal optimization (SMOreg) (Shevade et al., 2000) as the solver of quadratic programming. SMOreg implements the support vector machine for regression. PUK can generate better results as compared to other kernel functions (Radial Basis Function kernel, poly kernel, linear kernel), (Üstün et al., 2006; Zhang and Ge, 2013). More detailed descriptions of SMOreg can be obtained from Shevade et al. (2000). This retrieval algorithm implementation was achieved using Waikato Environment for Knowledge Analysis (WEKA) package (Frank et al., 2004; Holmes et al., 1994). The WEKA, as analysis and data mining (DM) software, has been used in many fields, such as biology (Zhang and Ge, 2013), image analysis (Vieira et al., 2012), medicine (Hester et al., 2006) and others. In this study, all running parameters of PUK and SMOreg were set as defaults in WEKA Version 3.6.13. The input data have ten parameters including Tb19V, Tb19H, Tb37V, Tb37H, Tb85V (or Tb91V), Tb85H (or Tb91H), meteorological station location and terrain parameter (latitude, longitude and elevation) and the in situ measured snow depth. The output of the SVR snow-depth retrieval algorithm is the predicted snow depth.

Step 6. Training dataset selection

The accuracy of the estimation depends mainly on the training data. Before using this retrieval algorithm, determining a suitable size and selection rule for training samples is critical for constructing a retrieval sub-model with higher accuracy.

We select the dataset over bare land in stage ii (2001 to 2006) as a trial dataset to confirm the appropriate number of training samples. Fig. 4 shows the accuracy through correlation coefficient (R), mean absolute error (MAE), and root mean squared error (RMSE) with evaluation datasets. The accuracy indexes (R, MAE and RMSE) become stable when the number of training sample is approximately 15,000 (Fig. 4). When the number of training sample increases from 2000 to 16,000, the R of the SVR snow-depth retrieval algorithm with evaluation datasets increases from 0.74 to 0.81 (Fig. 4). For MAE and RMSE, it decreases with increasing numbers of training sample datasets.

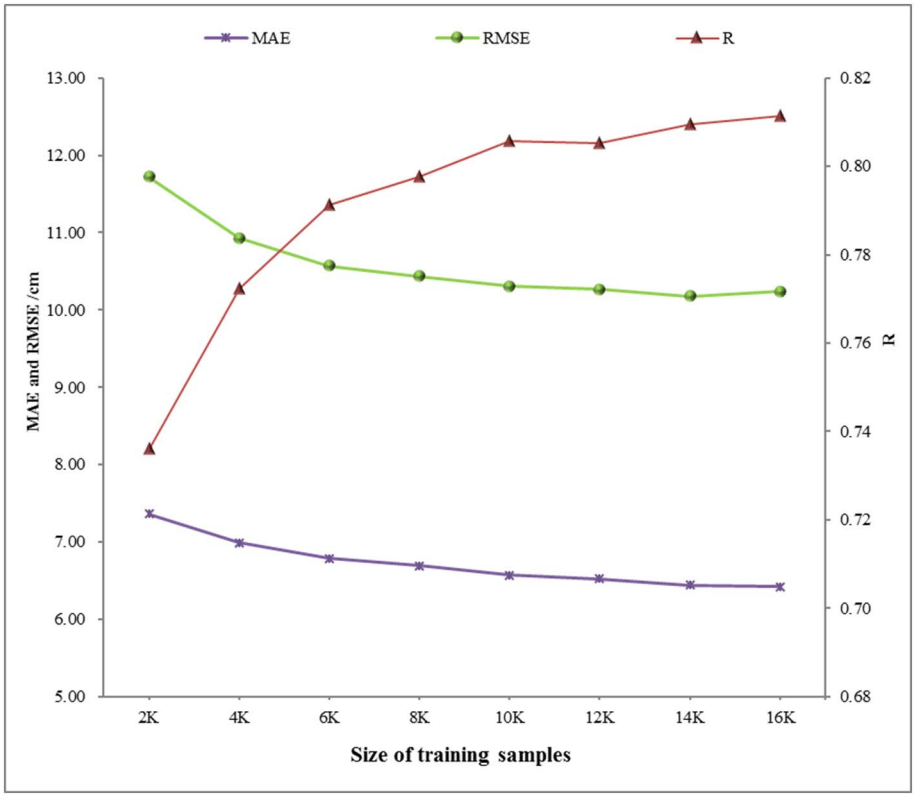

Fig. 4. Trend of R (correlation coefficient), MAE (mean absolute error) and RMSE (root mean squared error) with increase of training samples size. K means one thousand.

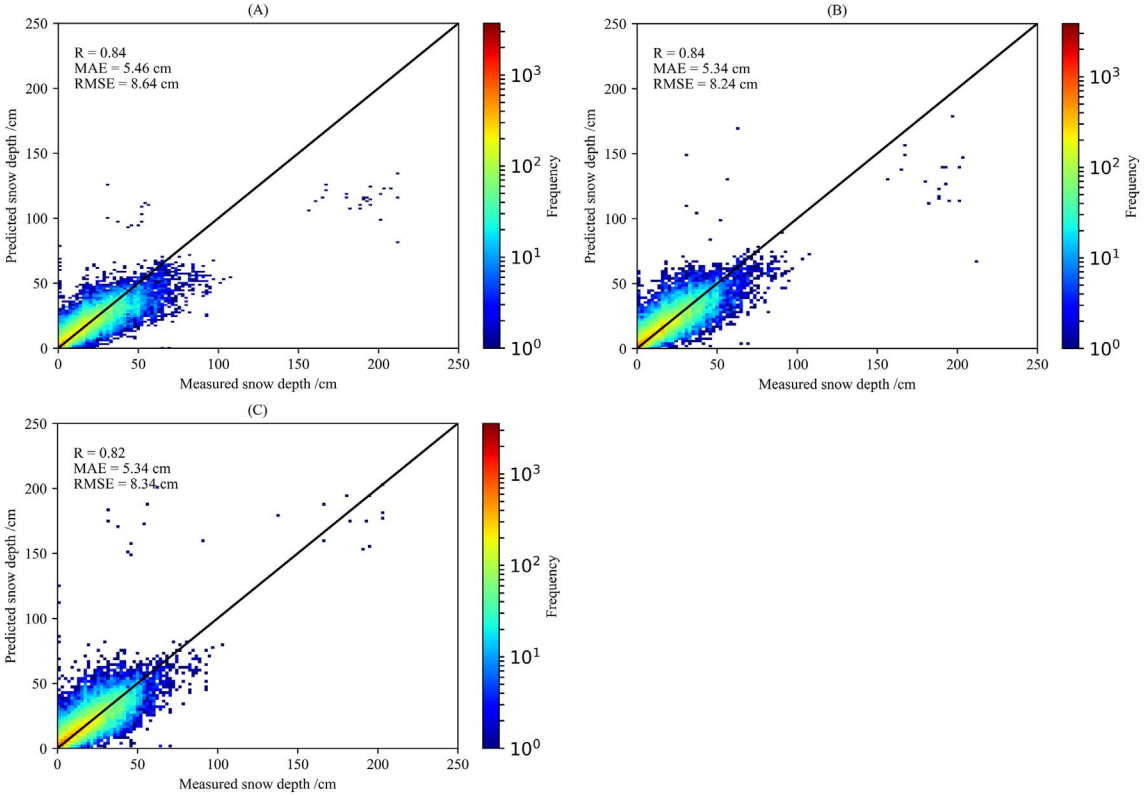

Fig. 5. The color-density scatterplots of the predicted snow depth and the measured snow depth for three selecting rules of training sample. A, B and C show the retrieval results for Test1, Test2 and Test3 using evaluation datasets, respectively. The color indicates point frequency.

Snow depth ranges from 0 to 250 cm in our study region. We divided snow depth (SD) into three layers: layer1 ($0 \leq SD < 50$), layer2 ($50 \leq SD < 100$) and layer3 ($SD \geq 100$). To explore the quantitative proportion of the three layers and seek a more appropriate selection rule, we only conducted three rules for training sample selection. In this section, all training and evaluation data is taken in stage ii (2007–2012) over bare-land. In the first rule (Test1), we selected 14,000 samples from the whole data. For the second rule (Test2), we selected 12,000 samples from the layer1 data directory while layer2 and layer3's quantitative proportion is only half of the corresponding layer data directory. The third rule (Test3) is almost same as the second rule, but layer2 and layer3's quantitative proportion is 2/3 of corresponding layer data directory. Note that all selections were made randomly and the remaining data of the dataset or each layer data directory were used as evaluation dataset.

Compared with the other two tests (Fig. 5A and C), Test2's predicted snow depth almost distributed near the 1:1 line with high frequency and Test2 show the best performance with the highest R, the least MAE and RMSE. We found a few data away from the 1:1 line. Thus, we adopted the second rule for subsequent analysis and modeling. This training sample selection rule is different from Liang's rule (8000 is randomly selected) (Liang et al., 2015). The main reason is that these two datasets characteristics are different. The data used in this test have much deeper snow (> 100 cm), while snow depth data in Liang's test ranges from 0 to 80 cm.

4. Results

Snow depth estimates were implemented using the retrieval processes described in Section 3. In this study, SSM/I (2001–2006) and SSMIS (2007–2012) were taken as input satellite data. We built 12 snow-depth retrieval models for each PM sensor. Thus, we apply 24 models in this study. We presented the retrieval results with evaluation datasets from different snow-depth retrieval sub-models. Four accuracy indexes, such as R, mean absolute relative error (MARE), MAE, and RMSE were used to evaluate the accuracy of the predicted snow depth against the in situ measured snow depth (Section 4.1). Additionally, we conducted comparisons between the SVR snow-depth retrieval algorithm and four other snow-depth retrieval algorithms (Chang algorithm, SPD algorithm, ANN algorithm and an algorithm based on linear regression; see Section 4.2).

4.1. Results of snow depth retrieval algorithm

We built 24 snow-depth retrieval models for this study and measured their accuracy with R, MARE, MAE and RMSE (Table 4). The MAE and RMSE of forest and shrub are slightly worse than that of bare-land and prairie because higher vegetation could attenuate more microwave radiation scatter signal from snow (Table 4). Snow depth retrieved from PM brightness temperature data (SSM/I, SSMIS) exhibit varying accuracy for different land cover types and snow cover stages.

In most cases, the MARE of the models based on four land cover types in the stage ii for both phases, 2001–2006 and 2007–2012, is lower than it is in the other two stages, suggesting that the snow properties (grain size, density etc.) with lower fluctuation would deliver little error into estimated snow depth in stage ii (Fig. 6). Moreover, tendency of MAE and RMSE increase on each land cover types as time progresses (from stage i to iii). In snow cover stage i, snow-depth models based on four land cover types yielded smaller error compared with these in stage iii. This may be due to increasing snow grain size and snow density, and the snow becomes wetter during this defined ablation stage, iii. From October to November (stage i), fresh snow appears with lower snow density, smaller grain size and shallower snow depth. These snow properties are conducive to derive snow depth with higher accuracy, and permit the estimated snow depth with less error. However, once snow has compacted, metamorphosis results in the fluctuation of snow physical and dielectric properties during March to April (stage iii). Because of increasing snow density and grain size, more liquid water content may cause significant uncertainty (Dai et al., 2012; Josberger and Mognard, 2002). In this study, the snow cover year

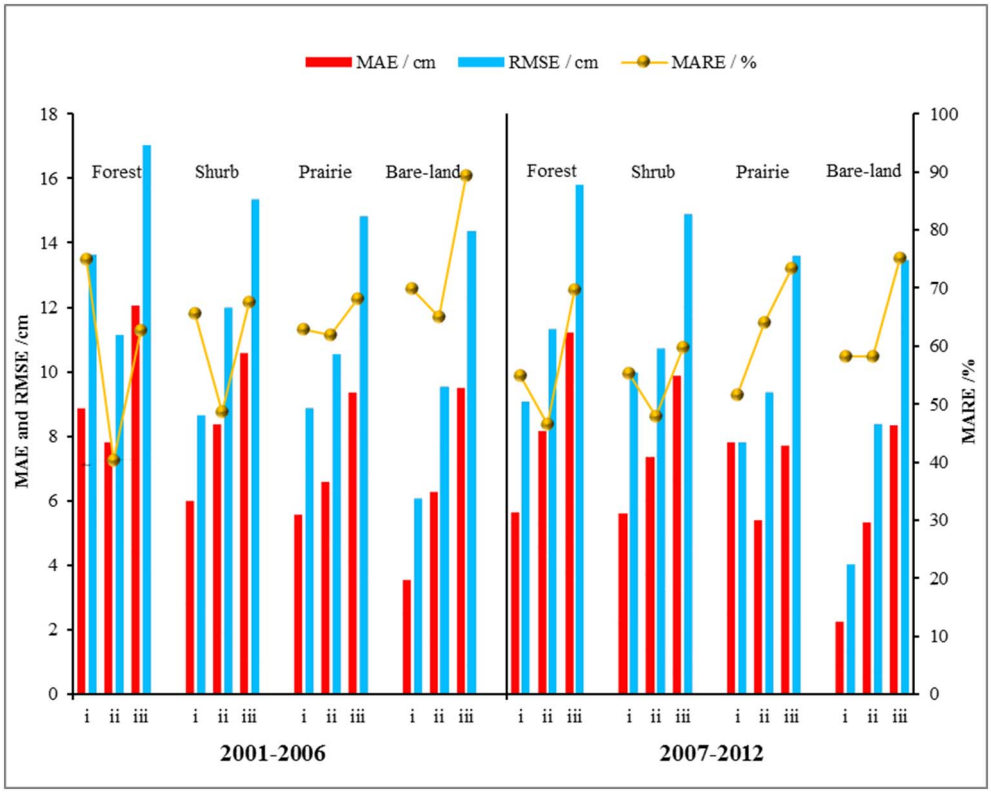

Fig. 6. The variation of the accuracy indexes (MARE, MAE and RMSE) based on three different snow cover stages over four kinds of land cover types.

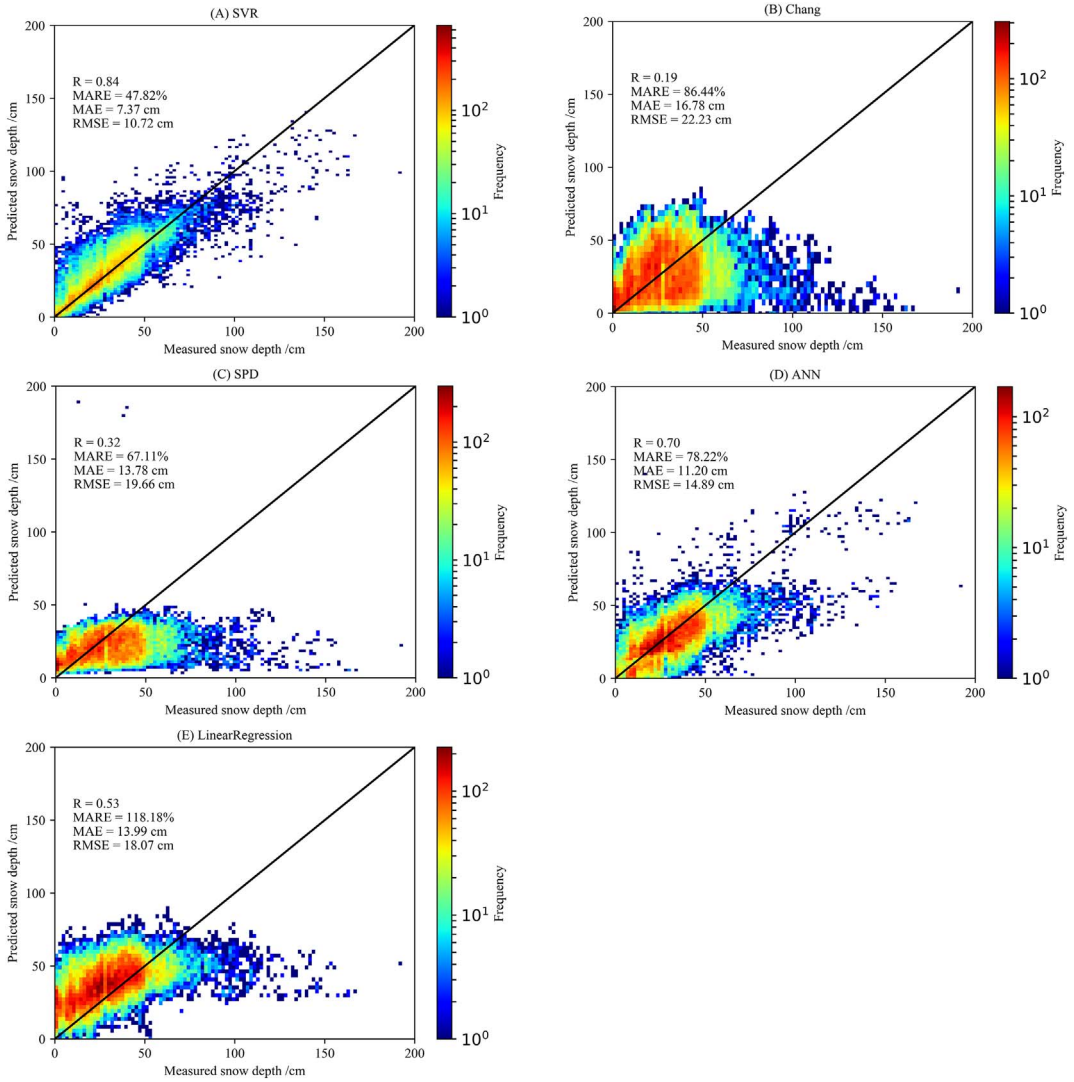

Fig. 7. The color-density scatterplot of the in situ measured and the retrieved snow depth from five retrieval algorithms. Additional comparisons are available in the Appendix A.

was divided into three snow cover stages to indirectly consider the evolution of the snow properties.

4.2. Comparison with previous algorithms

4.2.1. Comparison among the SVR snow-depth retrieval algorithm, Chang algorithm, SPD algorithms, ANN algorithm and linear regression algorithm

In this part, we used the in situ measured snow depth dataset and brightness temperature data in stage ii (for phase 2007–2012) over shrub land cover as an evaluation dataset.

The color-density scatterplot of the measured snow depth versus the retrieved snow depth of the Chang algorithm is presented in Fig. 7B. Fig. 7B also presents the accuracy, R (0.19), MARE (86.44%), MAE (16.78 cm) and RMSE (22.33 cm), obtained by application of the Chang algorithm (Chang et al., 1987).

$$SD = 1.59 \times (Tb18H - Tb36H) \quad (4)$$

SD is snow depth in cm. Tb18H and Tb36H are brightness temperature in horizontal polarization. Chang et al. (1987) developed the algorithm based on the difference of 18 and 36 GHz brightness temperature. In Eq. (4), we used the channel of 19 and 37 GHz to replace 18 and 36 GHz, respectively.

The accuracy of SPD retrieval algorithm was R = 0.32, MARE = 67.11%, MAE = 13.78 cm, and RMSE = 19.66 cm (Fig. 7C). Compared with Chang algorithm (Fig. 7B), the SPD algorithm (Fig. 7C) performed better, especially in layer1 (snow depth < 50 cm). This may be because the more brightness temperature channels that include snowpack information it uses, the better performance of the retrieval algorithm it would be. However, the SPD algorithm performance becomes worse when estimating deeper snow (snow depth > 50 cm). This result is same as in previous study (Liang et al., 2015). The SPD algorithm (Aschbacher, 1989; Tedesco et al., 2004) is based on the combination of 19 and 37 GHz vertical and horizontal brightness temperature.

$$SPD = [(Tb19V - Tb37V) + (Tb19V - Tb19H)] \quad (5)$$

$$SD = A_0 \times SPD - A_1 \quad (6)$$

The coefficients in Eq. (6) are the following: $A_0 = 0.68$, $A_1 = -0.67$.

Tedesco et al. (2004) uses Artificial neural networks (ANN) to construct snow-depth retrieval models. Input parameters, Tb19V, Tb19H, Tb37V, Tb37H, Tb85V (or Tb91V), Tb85H (or Tb91H), meteorological station location and terrain parameter (latitude, longitude and elevation) and the in situ measured snow depth, that is same as the SVR snow-depth retrieval algorithm and the output is the predicted snow depth. In training phase, the measured snow depth was used as input parameter, while the predicted snow depth as an output parameter in snow depth retrieval phase. The artificial neural networks is a multi-layer perception and is made up of one input layer, one output

layer and one or more hidden layers of neurons between the input and output layers (Tedesco et al., 2004). Interconnection is weighted to control the connection strength. Compared to our algorithm (Fig. 7A), ANN performance (Fig. 7D) become worse in any layers of snow depth with R from 0.84 to 0.70, MARE from 47.82% to 78.22%, MAE from 7.34 to 11.20 cm and RMSE from 10.72 to 14.89 cm. Previous studies also generated similar results. Using the support vector machine technique provides better performance than using the ANN algorithm (Liang et al., 2015; Xue and Forman, 2015). However, ANN performed better than the SPD algorithm and the Chang algorithm (Fig. 7B, C, D). Tedesco et al. (2004) also came to a similar conclusion. In this study, ANN was operated in WEKA with all running parameters as defaults in WEKA Version 3.6.13.

Linear regression is used in many applications (Frank et al., 2004; Hester et al., 2006; Rodrigo and Baker, 2009; Witten and Frank, 2005). It uses one or several parameters to construct a model for predicting results. Ten parameters (same as the SVR snow-depth retrieval algorithm) were used to build snow-depth retrieval model in this test. Parameters for the linear regression models were selected by the M5 method (Akaike, 1974), which performs a backward stepwise regression. The correlation coefficient (R) of the retrieved and measured snow depth is 0.53, and the MARE = 118.18%, MAE = 13.99 cm, RMSE = 18.07 cm (Fig. 7E).

Our proposed algorithm performed the best compared to the other four snow-depth retrieval algorithms. It had the highest R, least MARE, lowest MAE and RMSE (Fig. 7). We found great agreement between the predicted and the in situ measured snow depth from meteorological stations. Overestimation and underestimation is prevalent in the Chang algorithm, the SPD algorithm, the ANN algorithm, and the algorithm based on linear regression but less frequent in the proposed retrieval algorithm. Among the three linear methods (Chang algorithm, SPD algorithm, and an algorithm based on linear regression), the linear regression model yielded better results in deep snow. This may be because it uses additional parameters which include snow properties information to derive snow depth, and then the less error in estimated snow depth. Overall, nonlinear algorithms (ANN algorithm and SVR algorithm) have better performance than linear algorithms.

4.2.2. Comparison between the SVR snow-depth retrieval algorithm and Liang algorithm in Xinjiang, China

In this part, we do a comparison between the Liang algorithm (Liang et al., 2015) and the SVR snow-depth algorithm in Xinjiang, China. Liang et al. (2015) have demonstrated that the integrating PM data and reflectance data performs better than only using PM data. Thus, we compared the performance of these two snow depth retrieval algorithms only using PM data. In this study area, Xinjiang, China, we collected 56 meteorological stations from 2001 to 2012, including 30,558 valid snow depth records. As described in Liang et al. (2015), we randomly selected 8000 records as the training sample for Liang algorithm. The parameters of PUK and SMOreg in WEKA 3.6.13 as default are same as the proposed algorithm. The evaluation datasets for three land cover types (bare-land, shrub, and prairie), no forest type in this area, in stage ii (2007–2012) were used to evaluate the SVR snow-depth retrieval algorithm (model 18–20) and Liang algorithm. Different from the SVR snow-depth retrieval algorithm, the input parameters of Liang algorithm only have Tb in two channels, which is Tb19V, Tb19H, Tb37V, and Tb37H.

Compared with Liang algorithm (Fig. 8B; D; F), overall, the SVR snow-depth retrieval algorithm (Fig. 8A; 8C; 8E) for three land cover types have better performance. Especially, the accuracy of these two algorithm in deeper snow (> 50 cm), the SVR snow-depth retrieval algorithm generated snow depth values with high accuracy (Fig. 8A–D). For bare-land land cover, the proposed algorithm (Fig. 8A) made more accurate results with higher R (from 0.79 to 0.76), less MAE (from 3.24 to 2.16 cm) and RMSE (from 5.27 cm to 4.40 cm). The reason of these differences may be due to the variation of land cover type and snow cover stage in the SVR snow-depth retrieval algorithm, and thus the impact of variation of land cover types and snow cover stages will be discussed in Section 4.3. In addition, the size of evaluation dataset for shrub is only 347 records and the snow depth range from 0 to 15 cm. In this land cover type, shrub, these two snow depth retrieval algorithms almost have similar performance (Fig. 8E; F).

4.3. The impact of different land cover types and snow cover stages on snow depth retrieval

To test the impacts of land cover types and snow cover stages on snow-depth retrieval process, we made five evaluation tests with five datasets (V1 - V5). V1 is for bare-land in stage ii (2001–2006); V2 and V3 is in stage ii (2001–2006) for forest cover type; V4 and V5 is in stage iii (2001–2006) for bare-land type (Table 5). We used three different evaluation datasets (V1, V3, and V5) to evaluate the snow-depth retrieval model 8. The other evaluation datasets (V2 and V4) were used to evaluate retrieval model 5 and model 12, respectively. The training dataset for bare-land type in stage ii (2001–2006) was used to construct retrieval model 8.

For the impact of the variation of land cover types, V2 and V3 were used to evaluate model 5 and model 8, respectively (Fig. 9b and c). V3 yielded poorer performance with lower correlation coefficient (from 0.79 to 0.35), higher RMSE (from 11.16 to 21.55 cm), higher MARE (from 40.20% to 55.59%) and MAE (from 7.80 to 15.84 cm). V2 has a better agreement between the estimated and the measured snow depth, however, the V3 shows that snow depth was underestimated across measured ranges (Fig. 9b and c). Vegetation overlaying snow attenuates its microwave scatter signal. Every land cover type has its specific snow radiation attenuation principle. Previous studies also show that estimating snow depth benefits from considering land cover types effects (Che et al., 2016; Liang et al., 2015; Vander Jagt et al., 2013; Yu et al., 2012).

For the impact of stage variation, we used V4 and V5 to evaluate model 12 and model 8, respectively (Fig. 9d and e). Deeper snow were underestimated, shallow snow is overestimated, and all accuracy index were worse in test V5 (Fig. 9e). This demonstrated that snow density and grain size are significant variable from stage to stage, and thus estimating snow depth and snow water equivalent may benefit from considering snow evolution. (Che et al., 2016; Dai et al., 2012; Foster et al., 2005)

5. Discussion

We noted that several parameters are needed as input or auxiliary data to derive snow depth (Eq. (2)). In this study, all figures (additional figures available in the Appendix A, Fig. A1–A3) show that points are frequently distributed around the 1:1 line. However, there are a number of points away from that line. Although we considered a number of parameters associated with snow physical properties in the snow-depth retrieval process and the SVR snow-depth retrieval algorithm show the best performance with high accuracy, we still found snow depth underestimation and overestimation with respect to the in situ measured snow depth. Over and underestimation of snow depth is inevitable because of the limited data sources for higher resolution PM data.

There is representativeness error in modeling snow-depth. The PM data resolution is $25 \times 25\,km^2$, however, snow depth was measured over a limited area (Bulygina et al., 2011). In one pixel, the scope of $25 \times 25\,km^2$, snow properties (snow water, density, and grain size) present extensive heterogeneity. In most cases, one pixel only has one measured site. To be exact, using one point snow information to stand for one pixel is not appropriate. Huang et al. (2016) quantified the representativeness error of point-scale ground-based solar radiation measurements. Point measures are highly representative if snow depth varies smoothly temporally and spatially (Che et al., 2016). Vander Jagt et al. (2013) investigated the effect of spatial variability on the

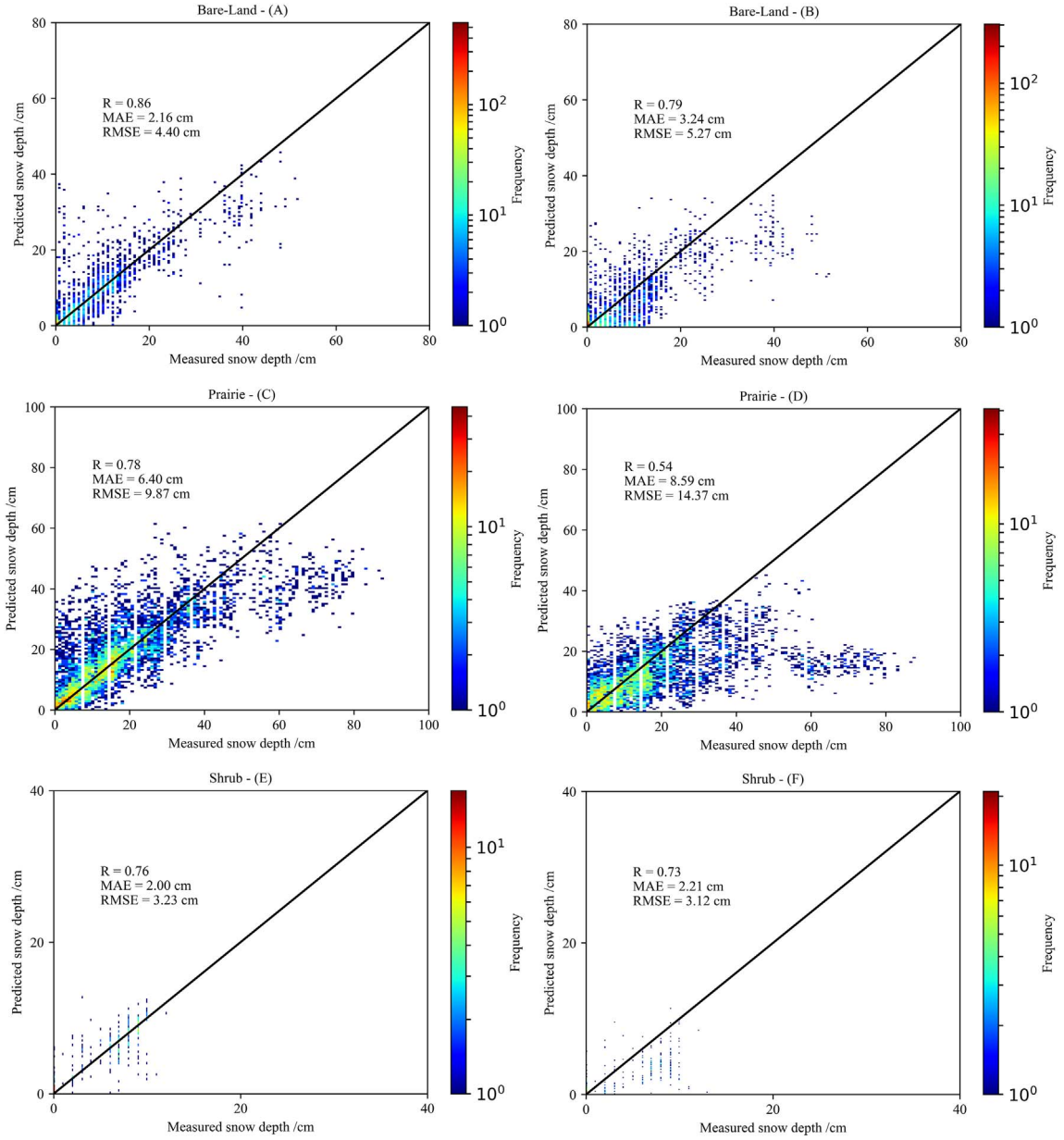

Fig. 8. The color-density scatterplot of the in situ measured and the retrieved snow depth from Liang algorithms and the proposed algorithm for three land cover types.

Table 5
Data description and accuracy of five test for the impact of different land cover type and snow cover stage on snow depth retrieval.

	Index	V1 (a)	V2 (b)	V3 (c)	V4 (d)	V5 (e)
Data information	Land Cover	Bare-land	Forest	Forest	Bare-land	Bare-land
	Snow cover stage	ii	ii	ii	iii	iii
Results	R	0.79	0.79	0.35	0.75	0.65
	MARE/%	65.08	40.20	55.59	89.36	117.33
	MAE/cm	6.26	7.80	15.84	9.51	17.78
	RMSE/cm	9.54	11.16	21.55	14.36	23.23

sensitivity of PM brightness temperature and found that PM brightness temperature remains sensitive to the sub-pixel mean snow depth. Generally, snow properties are heterogeneous across temporal and spatial scales. The limitation of the microwave technique is that the spatial resolution is too coarse for detailed environmental applications including regional weather prediction. These analyses suggest that the downscaling technique and higher spatial resolution PM data may draw attention to derive snow depth and snow water equivalent with high accuracy (Li et al., 2015; Vander Jagt et al., 2013).

Furthermore, the spatial coverage of study area, over the Eurasian continent, spans from 20°N to 80°N and from 20°E to 180°E (and from 170°W to 180°W), and the topography is variable and complex. Because complex terrain characteristics could affect the distribution and scatter signal of snow, there are considerable limitation to acquiring snow scatter signals from remote sensors. Previous studies reach a similar conclusion (Mizukami and Perica, 2012; Revuelto et al., 2014; Smith and Bookhagen, 2016; Tedesco and Narvekar, 2010). In such cases, snow does not exhibit completely homogenous properties, so the scatter signals correlate poorly with snow depth. This phenomenon suggests heterogeneous scatter signal could disturb the snow depth modeling.

6. Conclusions

This study tests a support vector regression (SVR) technique for estimating snow depth using passive microwave (PM) remote data and

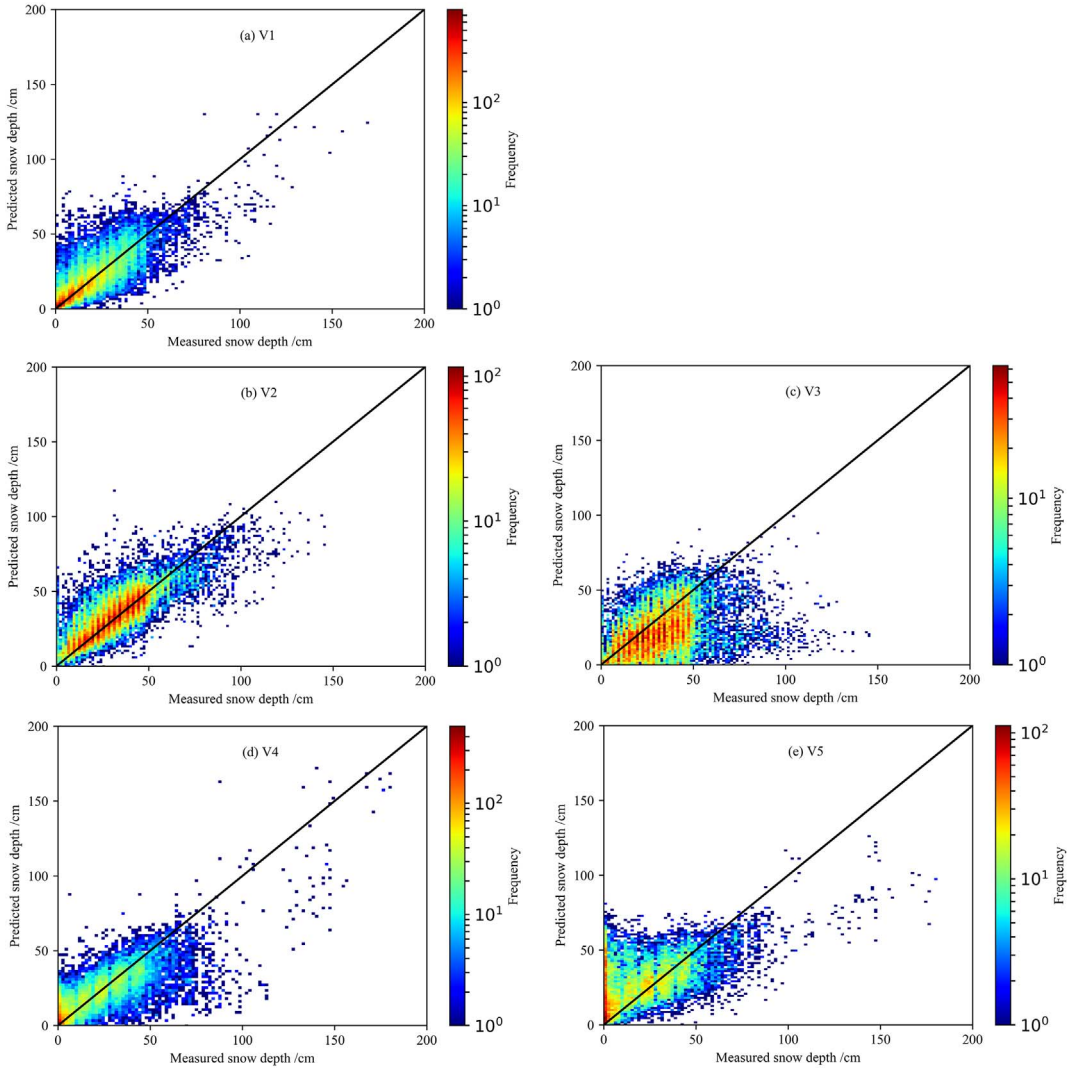

Fig. 9. The color-density scatterplots of the predicted and the measured snow depth. The meaning of letters (a – e) refer to Table 5.

meteorological station measured data. Three snow cover stages and four land cover types divided this SVR snow-depth retrieval algorithm into 12 snow-depth retrieval models for each phase. We established 24 snow-depth retrieval models, with PM brightness temperatures such as Tb19H, Tb19V, Tb37H, Tb37V, Tb85H (or Tb91H), Tb85V (or Tb91V), location and terrain parameters (latitude, longitude, elevation) as input data and land cover as auxiliary data, through an artificial intelligence approach. We compared the SVR snow-depth algorithm with other popular snow-depth retrieval algorithms. The snow-depth retrieval model based on SVR technique for different conditions show the best performance. The developed SVR snow-depth retrieval algorithm with more parameters associated with snow properties was found to be an efficient and effective algorithm for retrieving snow depth over various scales.

The saturation effects (Tedesco and Narvekar, 2010) associated with snowpack is difficult to overcome in using PM remote sensing data. In general, the threshold value is set about 60 cm, and the threshold has up to about 150 cm after operating the SVR snow-depth retrieval algorithm (more results not shown). The advantage of the proposed algorithm are improved the retrieval accuracy of snow depth and decreased the impact of saturation effects on estimating snow depth and snow water equivalent. One possible explanation for the improvement in saturation effects is that the SVR technique is sensitive in both shallow and deep snow (Xue and Forman, 2015). Another reason may be that the proposed retrieval algorithm makes use of the available input parameters that is the Tb and ancillary data rather than Tb differences (Tedesco and Narvekar, 2010). This study also suggested the vegetation is arguably a problem when using PM brightness temperature to estimate snow depth. This is consistent with the findings of previous studies (Vander Jagt et al., 2013). The performance of 12 models on four land cover types and three snow cover stages for each phase is worse when the land cover types are forest and shrub, compared to bare-land and prairie land cover types. Moreover, when deep snowpack with little metamorphosis or infrequent freeze-thaw cycles, which indicate that snow properties show small fluctuations, the SVR snow-depth retrieval algorithm performed better with lower error.

Because of these deficiencies and limitations (e.g. overestimate, underestimate, complex terrain and vegetation), further efforts should

be made to explore the relationship between snowpack and other variables, such as reflectance (Charrois et al., 2016; Liang et al., 2015) and terrain relief (Gharaei-Manesh et al., 2016; Smith and Bookhagen, 2016). To make use of the SVR approach available in WEKA and estimate snow depth with higher accuracy, more effort should also be devoted to optimize parameters (Forman and Reichle, 2015). All the running parameters of SVR method were set as defaults in WEKA. Finally, we would apply this algorithm to retrieve snow water equivalent and snow depth over the Northern Hemisphere.

Acknowledgments

The authors are very grateful for the constructive comments and suggestions from anonymous reviewers. This study was funded by the National Natural Science Foundation of China (grant nos. 91325202) and National Key Scientific Research Program of China (grant no. 2013CBA01802) funded.

Appendix A

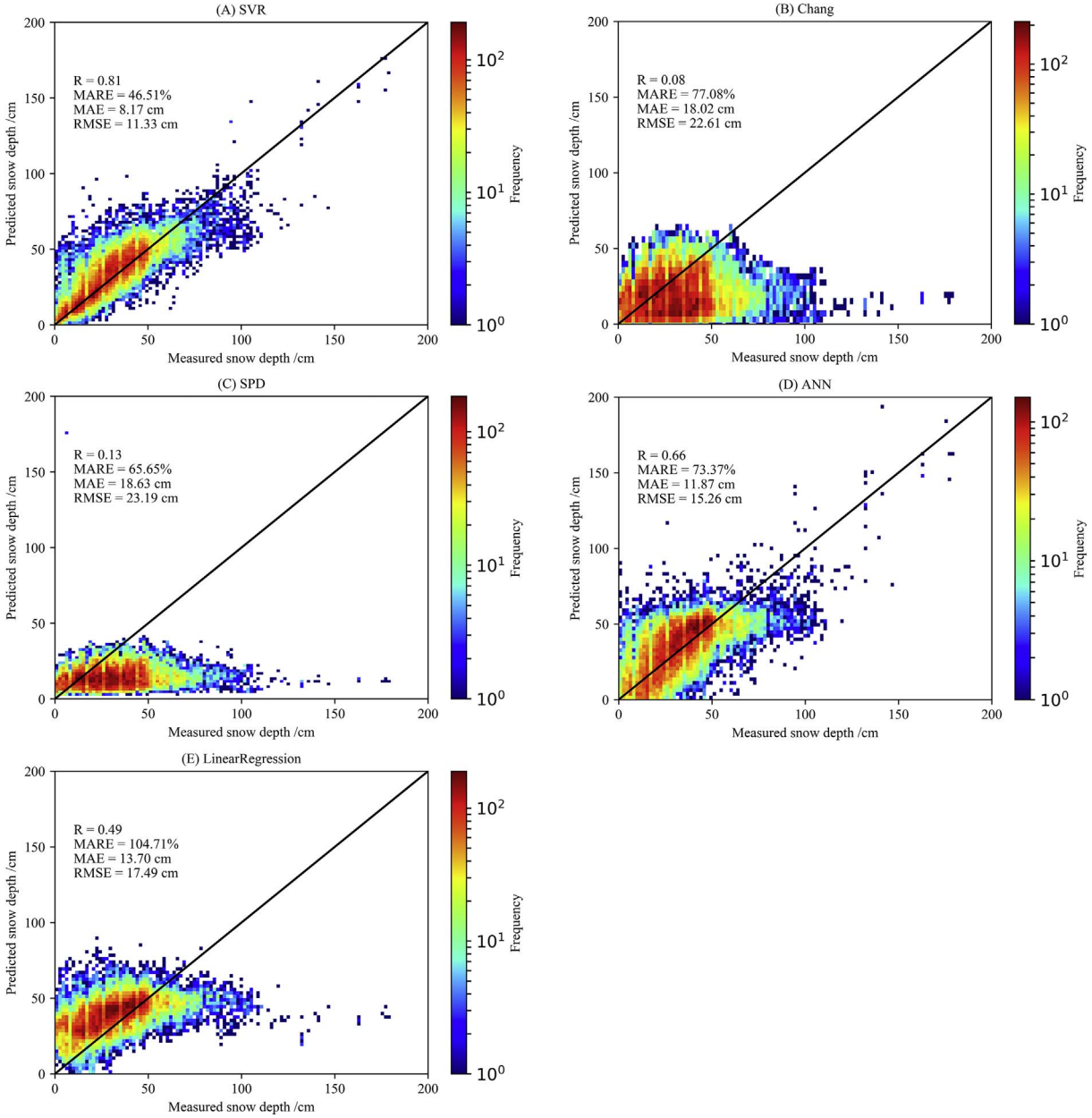

Fig. A1. The color-density scatterplot of the in situ measured and retrieved snow depth from fiver retrieval algorithm, the algorithm based on SVR technique (A), the Chang algorithm (B), the SPD algorithm (C), the ANN algorithm (D), and the algorithm based on linear regression technique (E), on stage ii (2007–2012) and forest.

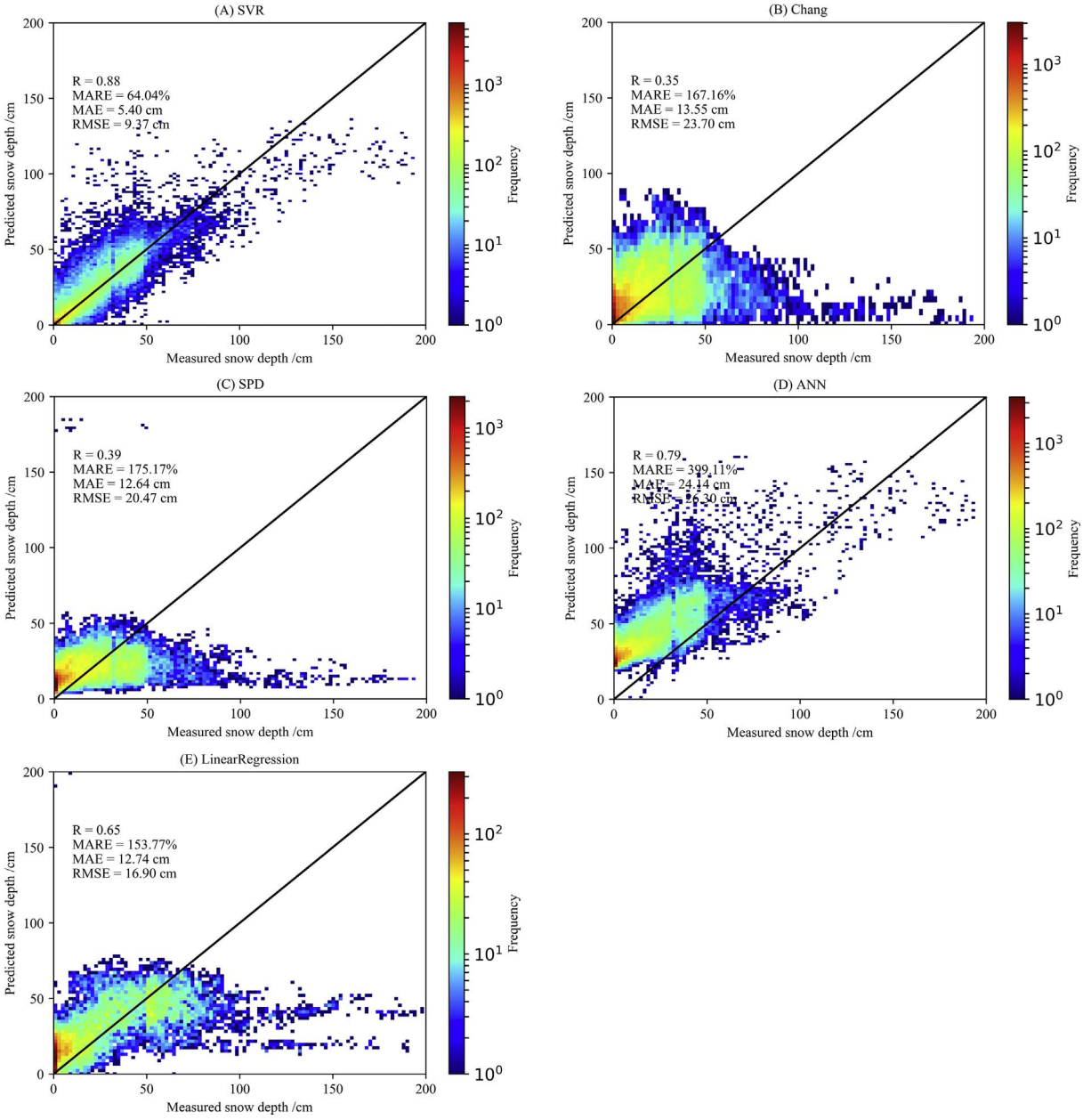

Fig. A2. The color-density scatterplot of the in situ measured and retrieved snow depth from fiver retrieval algorithm, the algorithm based on SVR technique (A), the Chang algorithm (B), the SPD algorithm (C), the ANN algorithm (D), and the algorithm based on linear regression technique (E), on stage ii (2007–2012) and prairie.

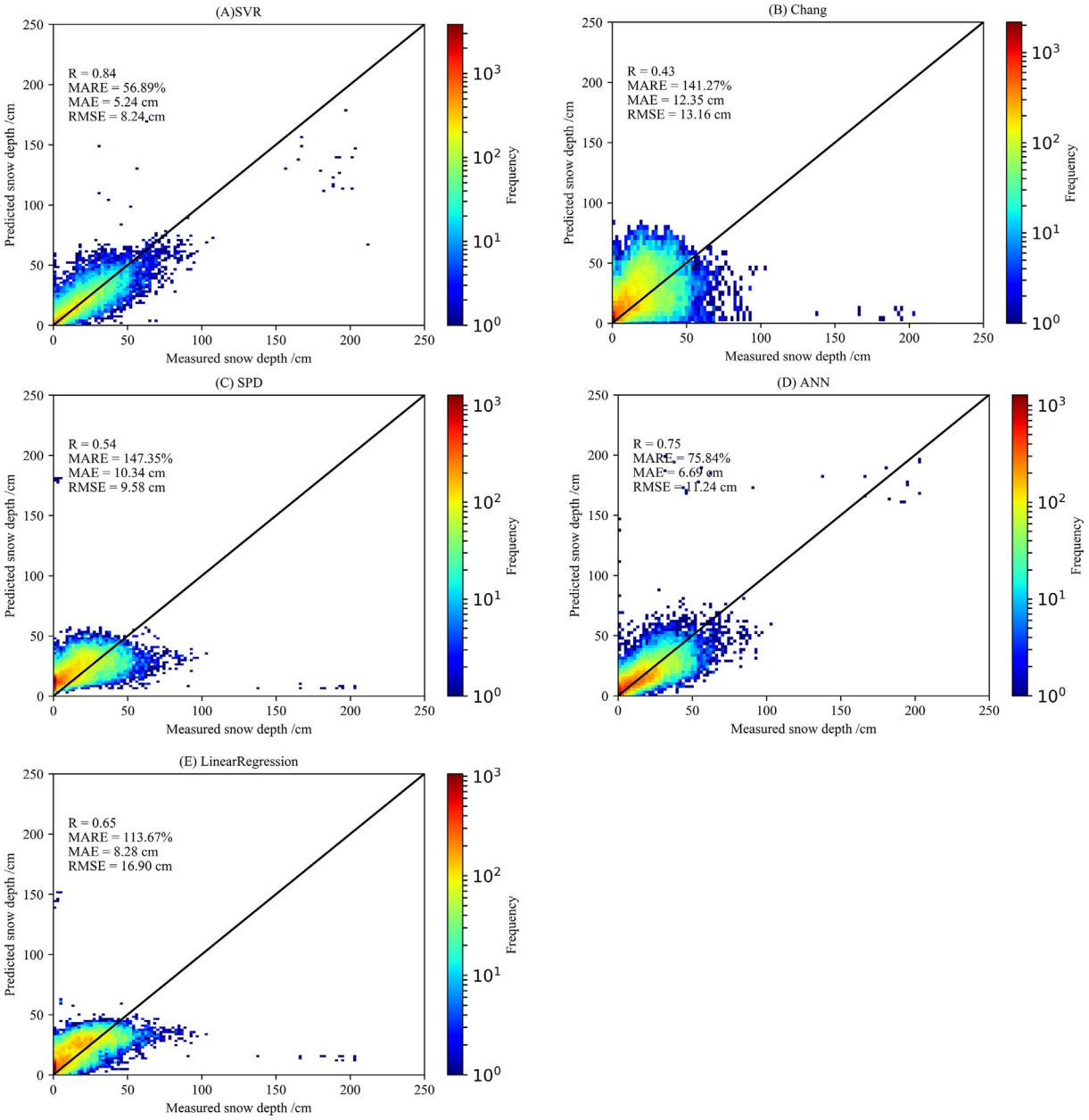

Fig. A3. The color-density scatterplot of the in situ measured and retrieved snow depth from fiver retrieval algorithm, the algorithm based on SVR technique (A), the Chang algorithm (B), the SPD algorithm (C), the ANN algorithm (D), and the algorithm based on linear regression technique (E), on stage ii (2007–2012) and bare-land.

Table B
Land cover type reclassification of the IGBP classification system.

Class	IGBP	Regroup
0	Water	Water
1	Evergreen needle leaf forest	Forest
2	Evergreen broad leaf forest	
3	Deciduous needle leaf forest	
4	Deciduous broad leaf forest	
5	Mixed forest	
6	Closed shrub lands	Shrub
7	Open shrub lands	
8	Woody savannas	Prairie (grassland)
9	Savannas	
10	Grasslands	
11	Permanent wetlands	

12	Croplands	Bare-Land
13	Urban and built-up	
14	Cropland/natural vegetation mosaic	
15	Snow and ice	
16	Barren or sparsely vegetated	
254	Unclassified	Unclassified

References

Akaike, H., 1974. New look at statistical-model identification. IEEE Trans. Autom. Control AC19, 716–723.

Amante, C., Eakins, B.W., 2009. ETOPO1 1 Arc-minute Global Relief Model: Procedures, Data Sources and Analysis. US Department of Commerce, National Oceanic and Atmospheric Administration, National Environmental Satellite, Data, and Information Service, National Geophysical Data Center, Marine Geology and Geophysics Division Colorado.

Armstrong, R.L., Brodzik, M.J., 1995. An earth-gridded SSM/I data set for cryospheric studies and global change monitoring. Adv. Space Res. 16, 155–163.

Armstrong, R.L., Brodzik, M.J., 2002. Hemispheric-scale comparison and evaluation of passive-microwave snow algorithms. Ann. Glaciol. 34, 38–44.

Armstrong, R.L., Knowles, K.W., Brodzik, M.J., Hardman, M.A., 2008. DMSP SSM/I Pathfinder Daily EASE-Grid Brightness Temperatures. National snow and ice data center. Digital media, Boulder, Colorado USA.

Aschbacher, J., 1989. Land Surface Studies and Atmospheric Effects by Satellite Microwave Radiometry. (na).

Basak, D., Pal, S., Patranabis, D.C., 2007. Support vector regression. Neural Inf. Process. Lett. Rev. 11, 203–224.

Bi, Y.B., Xie, H.J., Huang, C.L., Ke, C.Q., 2015. Snow cover variations and controlling factors at Upper Heihe River Basin, Northwestern China. Remote Sens. 7, 6741–6762.

Bin, C., 2013. Improvement of Passive Microwave Snow Algorithm Over Qinghai-Tibet Plateau. Shijiazhuang University of Economics, Shijiazhuang.

Brodzik, M.J., Knowles, K., 2002. EASE-Grid: A Versatile Set of Equal-Area Projections and Grids.

Brown, R.D., Mote, P.W., 2009. The response of northern hemisphere snow cover to a changing climate*. J. Clim. 22, 2124–2145.

Brown, R., Robinson, D., 2011. Northern hemisphere spring snow cover variability and change over 1922–2010 including an assessment of uncertainty. Cryosphere 5, 219–229.

Bulygina, O.N., Groisman, P.Y., Razuvaev, V.N., Korshunova, N.N., 2011. Changes in snow cover characteristics over Northern Eurasia since 1966. Environ. Res. Lett. 6, 045204.

Chang, A., Foster, J., Hall, D., 1987. Nimbus-7 SMMR derived global snow cover parameters. Ann. Glaciol. 9, 39–44.

Charrois, L., Cosme, E., Dumont, M., Lafaysse, M., Morin, S., Libois, Q., Picard, G., 2016. On the assimilation of optical reflectances and snow depth observations into a detailed snowpack model. Cryosphere 10, 1021–1038.

Che, T., 2006. Study on Passive Microwave Remote Sensing of Snow and Snow Data Assimilation Method. Cold and Arid Regions Environmental and Engineering Research Institute, CAS, In, Lanzhou.

Che, T., Xin, L., Jin, R., Armstrong, R., Zhang, T., 2008. Snow depth derived from passive microwave remote-sensing data in China. Ann. Glaciol. 49, 145–154.

Che, T., Li, X., Jin, R., Huang, C., 2014. Assimilating passive microwave remote sensing data into a land surface model to improve the estimation of snow depth. Remote Sens. Environ. 143, 54–63.

Che, T., Dai, L., Zheng, X., Li, X., Zhao, K., 2016. Estimation of snow depth from passive microwave brightness temperature data in forest regions of Northeast China. Remote Sens. Environ. 183, 334–349.

Cohen, J., Entekhabi, D., 2001. The influence of snow cover on northern hemisphere climate variability. Atmos. 39, 35–53.

Dai, L., Che, T., Wang, J., Zhang, P., 2012. Snow depth and snow water equivalent estimation from AMSR-E data based on a priori snow characteristics in Xinjiang, China. Remote Sens. Environ. 127, 14–29.

Dai, L., Che, T., Ding, Y., 2015. Inter-calibrating SMMR, SSM/I and SSMI/S data to improve the consistency of snow-depth products in China. Remote Sens. 7, 7212–7230.

Derksen, C., 2008. The contribution of AMSR-E 18.7 and 10.7 GHz measurements to improved boreal forest snow water equivalent retrievals. Remote Sens. Environ. 112, 2701–2710.

Derksen, C., LeDrew, E., Walker, A., Goodison, B., 2000. Influence of sensor overpass time on passive microwave-derived snow cover parameters. Remote Sens. Environ. 71, 297–308.

Derksen, C., Walker, A., Goodison, B., 2005. Evaluation of passive microwave snow water equivalent retrievals across the boreal forest/tundra transition of western Canada. Remote Sens. Environ. 96, 315–327.

Forman, B.A., Reichle, R.H., 2015. Using a support vector machine and a land surface model to estimate large-scale passive microwave brightness temperatures over snow-covered land in North America. IEEE J. Sel. Top. Appl. Earth Obs. Remote Sens. 8, 4431–4441.

Foster, J., Chang, A., Hall, D., 1997. Comparison of snow mass estimates from a prototype passive microwave snow algorithm, a revised algorithm and a snow depth climatology. Remote Sens. Environ. 62, 132–142.

Foster, J.L., Hall, D.K., Chang, A.T., Rango, A., Wergin, W., Erbe, E., 1999. Effects of snow crystal shape on the scattering of passive microwave radiation. IEEE Trans. Geosci. Remote Sens. 37, 1165–1168.

Foster, J.L., Sun, C., Walker, J.P., Kelly, R., Chang, A., Dong, J., Powell, H., 2005. Quantifying the uncertainty in passive microwave snow water equivalent observations. Remote Sens. Environ. 94, 187–203.

Frank, E., Hall, M., Trigg, L., Holmes, G., Witten, I.H., 2004. Data mining in bioinformatics using Weka. Bioinformatics 20, 2479–2481.

Friedl, M.A., Sulla-Menashe, D., 2011. Note to Users of MODIS Land Cover (MCD12Q1) Products. Report. (Accessed March, 2, 2014).

Friedl, M.A., Sulla-Menashe, D., Tan, B., Schneider, A., Ramankutty, N., Sibley, A., Huang, X., 2010. MODIS collection 5 global land cover: algorithm refinements and characterization of new datasets. Remote Sens. Environ. 114, 168–182.

G.Barry, R., Gan, T.Y., 2011. Snowfall and snow cover. In: The Global Cryosphere.

Gan, T.Y., Barry, R.G., Gizaw, M., Gobena, A., Balaji, R., 2013. Changes in North American snowpacks for 1979–2007 detected from the snow water equivalent data of SMMR and SSM/I passive microwave and related climatic factors. J. Geophys. Res. Atmos. 118, 7682–7697.

Gharaei-Manesh, S., Fathzadeh, A., Taghizadeh-Mehrjardi, R., 2016. Comparison of artificial neural network and decision tree models in estimating spatial distribution of snow depth in a semi-arid region of Iran. Cold Reg. Sci. Technol. 122, 26–35.

Goïta, K., Walker, A.E., Goodison, B.E., 2003. Algorithm development for the estimation of snow water equivalent in the boreal forest using passive microwave data. Int. J. Remote Sens. 24, 1097–1102.

Gong, G., Cohen, J., Entekhabi, D., Ge, Y., 2007. Hemispheric-scale climate response to Northern Eurasia land surface characteristics and snow anomalies. Glob. Planet. Chang. 56, 359–370.

Goodison, B., Rubinstein, I., Thirkettle, F., Langham, E., 1986. Determination of Snow Water Equivalent on the Canadian Prairies Using Microwave Radiometry. IAHS-AISH publication, pp. 163–173.

Goodrich, L., 1982. The influence of snow cover on the ground thermal regime. Can. Geotech. J. 19, 421–432.

Grippa, M., Mognard, N., Le Toan, T., Josberger, E., 2004. Siberia snow depth climatology derived from SSM/I data using a combined dynamic and static algorithm. Remote Sens. Environ. 93, 30–41.

Grody, N.C., Basist, A.N., 1996. Global identification of snowcover using SSM/I measurements. IEEE Trans. Geosci. Remote Sens. 34, 237–249.

Gunn, S.R., 1998. Support Vector Machines for Classification and Regression. ISIS Technical Report. pp. 14.

Hall, D.K., 1987. Influence of depth hoar on microwave emission from snow in northern Alaska. Cold Reg. Sci. Technol. 13, 225–231.

Hall, D.K., Frei, A., Déry, S.J., 2014. Remote Sensing of Snow Extent. John Wiley & Sons, Ltd.

Hallikainen, M.T., 1989. Microwave radiometry of snow. Adv. Space Res. 9, 267–275.

Hansen, M., DeFries, R., Townshend, J., Carroll, M., Dimiceli, C., Sohlberg, R., 2003. Global percent tree cover at a spatial resolution of 500 meters: first results of the MODIS vegetation continuous fields algorithm. Earth Interact. 7, 1–15.

Hester, T., Hughes, R., Sherrill, D.M., Knorr, B., Akay, M., Stein, J., Bonato, P., 2006. Using wearable sensors to measure motor abilities following stroke. In: International Workshop on Wearable and Implantable Body Sensor Networks (BSN'06). IEEE, pp. 4–8.

Holmes, G., Donkin, A., Witten, I.H., 1994. Weka: a machine learning workbench. In: Intelligent Information Systems, 1994. Proceedings of the 1994 Second Australian and New Zealand Conference on. IEEE, pp. 357–361.

Huang, W.-j., HUANG, Z., CUI, C.-x., FENG, Z.-m., LI, Q., WANG, L., 2007. Temporal and spatial distribution of Xinjiang snow density and its consequence. J. Glaciol. Geocryol. 29, 66–72.

Huang, G., Li, X., Huang, C., Liu, S., Ma, Y., Chen, H., 2016. Representativeness errors of point-scale ground-based solar radiation measurements in the validation of remote sensing products. Remote Sens. Environ. 181, 198–206.

Immerzeel, W.W., Van Beek, L.P., Bierkens, M.F., 2010. Climate change will affect the Asian water towers. Science 328, 1382–1385.

IPCC, A.R.5, 2013. In: Stocker, T., Qin, D., Platter, G.-K., Tignor, M.M.B., Allen, S.K., Boschung, J., Nauels, A., Xia, Y., Bex, C., Midgley, P.M. (Eds.), Climate Change 2013: The Physical Science Basis. Contribution of Working Group I to the Fifth Assessment Report of the Intergovernmental Panel on Climate Change. Cambridge University Press, Cambridge.

Josberger, E.G., Mognard, N.M., 2002. A passive microwave snow depth algorithm with a proxy for snow metamorphism. Hydrol. Process. 16, 1557–1568.

Kelly, R., 2009. The AMSR-E snow depth algorithm: description and initial results. J. Remote Sens. Soc. Jpn. 29, 307–317.

Kelly, R.E., Chang, A.T., Tsang, L., Foster, J.L., 2003. A prototype AMSR-E global snow area and snow depth algorithm. IEEE Trans. Geosci. Remote Sens. 41, 230–242.

Li, H.Y., He, Y.Q., Hao, X.H., Che, T., Wang, J., Huang, X.D., 2015. Downscaling snow cover fraction data in mountainous regions based on simulated inhomogeneous snow ablation. Remote Sens. 7, 8995–9019.

Liang, J., Liu, X., Huang, K., Li, X., Shi, X., Chen, Y., Li, J., 2015. Improved snow depth retrieval by integrating microwave brightness temperature and visible/infrared reflectance. Remote Sens. Environ. 156, 500–509.
MacKay, M., Seglenieks, F., Verseghy, D., Soulis, E., Snelgrove, K., Walker, A., Szeto, K., 2003. Modeling Mackenzie basin surface water balance during CAGES with the Canadian Regional Climate Model. J. Hydrometeorol. 4, 748–767.
Mizukami, N., Perica, S., 2012. Towards improved snow water equivalent retrieval algorithms for satellite passive microwave data over the mountainous basins of western USA. Hydrol. Process. 26, 1991–2002.
Revuelto, J., Lópezmoreno, J.I., Azorinmolina, C., Vicenteserrano, S.M., 2014. Topographic control of snowpack distribution in a small catchment in the central spanish pyrenees: intra- and inter-annual persistence. Cryosphere 8 (5), 1989–2006.
Robinson, D.A., Frei, A., 2000. Seasonal variability of northern hemisphere snow extent using visible satellite data. Prof. Geogr. 52, 307–315.
Rodrigo, M.M.T., Baker, R.S., 2009. Coarse-grained detection of student frustration in an introductory programming course. In: Proceedings of the Fifth International Workshop on Computing Education Research Workshop. ACM, pp. 75–80.
Romanov, P., Tarpley, D., 2007. Enhanced algorithm for estimating snow depth from geostationary satellites. Remote Sens. Environ. 108, 97–110.
Rosenfeld, S., Grody, N., 2000. Anomalous microwave spectra of snow cover observed from special sensor microwave/imager measurements. J. Geophys. Res. Atmos. 105, 14913–14925.
Rott, H., Aschbacher, J., 1989. On the use of satellite microwave radiometers for large-scale hydrology. IAHS-AISH publication 21–30.
Savoie, M.H., Armstrong, R.L., Brodzik, M.J., Wang, J.R., 2009. Atmospheric corrections for improved satellite passive microwave snow cover retrievals over the Tibet Plateau. Remote Sens. Environ. 113, 2661–2669.
Schimel, J.P., Bilbrough, C., Welker, J.M., 2004. Increased snow depth affects microbial activity and nitrogen mineralization in two Arctic tundra communities. Soil Biol. Biochem. 36, 217–227.
Shevade, S.K., Keerthi, S.S., Bhattacharyya, C., Murthy, K.R.K., 2000. Improvements to the SMO algorithm for SVM regression. IEEE Trans. Neural Netw. 11, 1188–1193.
Singh, P.R., Gan, T.Y., 2000. Retrieval of snow water equivalent using passive microwave brightness temperature data. Remote Sens. Environ. 74, 275–286.
Smith, T., Bookhagen, B., 2016. Assessing uncertainty and sensor biases in passive microwave data across High Mountain Asia. Remote Sens. Environ. 181, 174–185.
Smola, A., Vapnik, V., 1997. Support vector regression machines. Adv. Neural Inf. Proces. Syst. 9, 155–161.
Strahler, A., Sensing, C.F.R., Geography, D.O., University, B., Boston, M., 1999. MODIS Land Cover Product Algorithm Theoretical Basis Document (ATBD) Version 5.0.
Sturm, M., Schimel, J., Michaelson, G., Welker, J.M., Oberbauer, S.F., Liston, G.E., Fahnestock, J., Romanovsky, V.E., 2005. Winter biological processes could help convert arctic tundra to shrubland. Bioscience 55, 17–26.
Sturm, M., Taras, B., Liston, G.E., Derksen, C., Jonas, T., Lea, J., 2010. Estimating snow water equivalent using snow depth data and climate classes. J. Hydrometeorol. 11, 1380–1394.
Sun, N., Weng, F., 2008. Evaluation of special sensor microwave imager/sounder (SSMIS) environmental data records. IEEE Trans. Geosci. Remote Sens. 46, 1006–1016.
Tait, A., 1998. Estimation of snow water equivalent using passive microwave radiation data. Remote Sens. Environ. 64, 286–291.
Takala, M., Luojus, K., Pulliainen, J., Derksen, C., Lemmetyinen, J., Kärnä, J.-P., Koskinen, J., Bojkov, B., 2011. Estimating northern hemisphere snow water equivalent for climate research through assimilation of space-borne radiometer data and ground-based measurements. Remote Sens. Environ. 115, 3517–3529.
Tape, K., Sturm, M., Racine, C., 2006. The evidence for shrub expansion in northern Alaska and the Pan-Arctic. Glob. Chang. Biol. 12, 686–702.
Tedesco, M., Narvekar, P.S., 2010. Assessment of the NASA AMSR-E SWE product. IEEE J. Sel. Top. Appl. Earth Obs. Remote Sens. 3, 141–159.
Tedesco, M., Pulliainen, J., Takala, M., Hallikainen, M., Pampaloni, P., 2004. Artificial neural network-based techniques for the retrieval of SWE and snow depth from SSM/I data. Remote Sens. Environ. 90, 76–85.
Tedesco, M., Derksen, C., Deems, J.S., Foster, J.L., 2014. Remote sensing of snow depth and snow water equivalent. In: Remote Sensing of the Cryosphere, pp. 73–98.
Üstün, B., Melssen, W., Oudenhuijzen, M., Buydens, L., 2005. Determination of optimal support vector regression parameters by genetic algorithms and simplex optimization. Anal. Chim. Acta 544, 292–305.
Üstün, B., Melssen, W.J., Buydens, L.M., 2006. Facilitating the application of support vector regression by using a universal Pearson VII function based kernel. Chemom. Intell. Lab. Syst. 81, 29–40.
Vander Jagt, B.J., Durand, M.T., Margulis, S.A., Kim, E.J., Molotch, N.P., 2013. The effect of spatial variability on the sensitivity of passive microwave measurements to snow water equivalent. Remote Sens. Environ. 136, 163–179.
Vapnik, V., Golowich, S.E., Smola, A.J., 1997. Support vector method for function approximation, regression estimation and signal processing. In: Advances in Neural Information Processing Systems, pp. 281–287.
Veselov, V., 2002. PC archives of the state data holding and technology of their organization. Proc. RIHMI-WDC 170, 16–30.
Vieira, M.A., Formaggio, A.R., Rennó, C.D., Atzberger, C., Aguiar, D.A., Mello, M.P., 2012. Object based image analysis and data mining applied to a remotely sensed Landsat time-series to map sugarcane over large areas. Remote Sens. Environ. 123, 553–562.
Walker, A., Goodison, B., 1993. Discrimination of a wet snow cover using passive microwave satellite data. Ann. Glaciol. 17, 307–311.
Wang, W., Huang, X., Deng, J., Xie, H., Liang, T., 2015. Spatio-temporal change of snow cover and its response to climate over the Tibetan Plateau based on an improved daily cloud-free snow cover product. Remote Sens. 7, 169–194.
Welker, J., Fahnestock, J., Jones, M., 2000. Annual CO2 flux in dry and moist arctic tundra: field responses to increases in summer temperatures and winter snow depth. Clim. Chang. 44, 139–150.
Welling, M., 2004. Support Vector Regression. Department of Computer Science, University of Toronto, Toronto (Kanada).
Wentz, F.J., 2013. SSM/I version-7 calibration report. Remote Sens. Syst. Tech. Rep. 11012, 46.
Witten, I.H., Frank, E., 2005. Data Mining: Practical Machine Learning Tools and Techniques. Morgan Kaufmann.
Xue, Y., Forman, B.A., 2015. Comparison of passive microwave brightness temperature prediction sensitivities over snow-covered land in North America using machine learning algorithms and the advanced microwave scanning radiometer. Remote Sens. Environ. 170, 153–165.
Yu, H., Zhang, X., Liang, T., Xie, H., Wang, X., Feng, Q., Chen, Q., 2012. A new approach of dynamic monitoring of 5-day snow cover extent and snow depth based on MODIS and AMSR-E data from Northern Xinjiang region. Hydrol. Process. 26, 3052–3061.
Zhang, T., 2005. Influence of the seasonal snow cover on the ground thermal regime: an overview. Rev. Geophys. 43, 589–590.
Zhang, G., Ge, H., 2013. Support vector machine with a Pearson VII function kernel for discriminating halophilic and non-halophilic proteins. Comput. Biol. Chem. 46, 16–22.
Zhang, T., Osterkamp, T., Stamnes, K., 1996. Influence of the depth hoar layer of the seasonal snow cover on the ground thermal regime. Water Resour. Res. 32, 2075–2086.
Zhong, X., 2014. spatiotemporal variability of snow cover and the relationship between snow and climate change across the Eurasian continent. In: Lanzhou: Cold and Arid Regions Environmental and Engineering Research Institute, CAS.
Zhong, X., Zhang, T., Wang, K., 2014. Snow density climatology across the former USSR. Cryosphere 8, 785–799.